

# Statistical Variability of Dispersion in the Convective Boundary Layer: LPDM-LES Model Ensembles and Observations

Jeffrey C. Weil · Peter P. Sullivan · Edward G. Patton · Chin-Hoh Moeng

Received: date / Accepted: date

**Abstract** A Lagrangian particle dispersion model (LPDM) driven by velocity fields from large-eddy simulations (LESs) is used to determine the mean and variability of plume dispersion in a highly-convective planetary boundary layer (PBL). The total velocity of a “particle” is divided into resolved and unresolved or random (subfilter scale, SFS) velocities with the resolved component obtained from the LES and the SFS velocity from a Lagrangian stochastic model. This LPDM-LES model is used to obtain an ensemble of dispersion realizations for calculating the mean, rms deviation, and fluctuating fields of dispersion quantities. An ensemble of 30 realizations is generated for each of three source heights: surface, near-surface, and elevated. We compare the LPDM calculations with convection tank experiments and field observations to assess the realism of the results.

The overall conclusion is that the LPDM-LES model produces a realistic range of dispersion realizations and statistical variability (i.e., rms deviations) that match observations in this highly convective PBL, while also matching the ensemble-mean properties. This is true for the plume height or trajectory, vertical dispersion, and the surface values of the crosswind-integrated concentration (CWIC), and their dependence on downstream distance. One exception is the crosswind dispersion for an elevated source, which is underestimated by the model.

Other analyses highlighted important LPDM results on: 1) the plume meander and CWIC fluctuation intensity at the surface, 2) the applicability of a similarity theory for plume height from a surface source to only the very strong updraft plumes—not the mean height, and 3) the appropriate variation with distance of the mean surface CWIC and the lower bound of the CWIC realizations for a surface source.

---

J. C. Weil  
Cooperative Institute for Research in Environmental Sciences, University of Colorado, Boulder, CO 80309  
USA  
E-mail: weil@ucar.edu

P.P. Sullivan · E.G. Patton · C.-H. Moeng  
National Center for Atmospheric Research, P.O. Box 3000, Boulder, CO 80307 USA

**Keywords** Concentration statistics · Convective boundary layer · Dispersion · Lagrangian particle model · Large eddy simulation · Turbulence

## 1 Introduction

Atmospheric dispersion is highly variable especially in a convective boundary layer (CBL) where large-scale updrafts and downdrafts lead to substantial plume “meandering”. For an elevated source, the meander is most significant in light winds and causes ground-level concentrations to vary essentially between “in-plume” peaks and the zero ambient level. The resulting concentration fluctuations are large and can be characterized by their root-mean-square (rms) value  $\sigma_c$  or the fluctuation intensity  $\sigma_c/C$ , where  $C$  is the ensemble-mean concentration. In the CBL, the  $\sigma_c/C$  at the surface typically ranges from 1 to 10 and possibly greater for short averaging times ( $< 1$  hr) and short downstream distances ( $\leq 5$  km) (Lewellen and Sykes, 1986; Mylne and Mason, 1991; Sykes, 1988), thus leading to a large uncertainty in the concentration. Knowledge of the uncertainty is important for predicting the peak concentrations of toxic materials, estimating pollutant exceedance probabilities, and evaluating dispersion models for  $C$ .

To determine the statistics of dispersion properties, one needs an ensemble of dispersion realizations collected under the same conditions. Some field experiments have been conducted for this purpose, but the generation of an ensemble is difficult to do “outdoors” because the same meteorology does not repeat with sufficient frequency. Another way of building an ensemble is with laboratory experiments. Deardorff and Willis (1984, 1988) did this using a convection tank to study concentration fluctuations in a simulated CBL. They obtained  $\sigma_c/C$  profiles and concentration probability distributions, finding a clear dependence of  $\sigma_c/C$  on source buoyancy, but the number of repetitions was small ( $< 10$ ). Snyder et al (2002) and Weil et al (2002) repeated some of their experiments using a system that permitted a much greater number of plume cross-section repeats ( $\simeq 350$  to 415) and produced more reliable statistics. Although these experiments were indeed useful and enlightening, they were limited to strong convection with no mean wind shear.

Numerical models exploiting large-eddy simulations (LESs) of the planetary boundary layer (PBL) offer another more general method for studying the statistical variability in dispersion by allowing for a range of PBL forcings (mean wind, surface heat flux, etc.). John Wyngaard was an early advocate of this approach in particular for studying the concentration variance problem (Wyngaard, 1984). He termed the variance  $\sigma_f^2$  in the time-averaged value  $\bar{f}$  of some property  $f$  about its ensemble-mean value  $\langle f \rangle$ , the “inherent uncertainty” in  $f$ ; i.e.,  $\sigma_f^2 = \langle (\bar{f} - \langle f \rangle)^2 \rangle$ . For a stationary and ergodic process, the  $\sigma_f^2$  is given by

$$\sigma_f^2 = \frac{2\langle f'^2 \rangle \tau_i}{T_{av}}, \quad (1)$$

for  $T_{av} \gg \tau_i$ , where  $T_{av}$  is the averaging time,  $\tau_i$  is the integral time scale of the process, and  $\langle f'^2 \rangle$  is the ensemble variance (Lumley and Panofsky, 1964).

Wyngaard was well aware of the large variances in turbulence quantities especially in the CBL surface layer and the need for long averaging times to reduce the uncertainty (Wyngaard, 1973). From his LES research with Moeng (e.g., Moeng and Wyngaard, 1988), he understood the capabilities of LES and its fidelity in simulating PBL turbulence. Thus, his push for LES in tackling the concentration variance problem was justified and supported by the success of Lamb (1978, 1982) in simulating mean concentration fields in the CBL using

a Lagrangian particle dispersion model (LPDM) driven by LES fields. Wyngaard also was a strong advocate for studying the role of inherent uncertainty in air quality model evaluation. His influence helped stimulate several workshops on this topic and was manifested in workshop reports and recommendations (e.g., Fox, 1984; Weil, 1985; Weil et al, 1992).

Following Lamb’s pioneering work, there were a number of LES-based numerical studies of dispersion in the CBL (Henn and Sykes, 1992; Nieuwstadt, 1992; Dosio et al, 2003; Weil et al, 2004; Dosio and de Arellano, 2006, (hereafter DdA06)). Most of them investigated the mean dispersion properties finding generally good agreement between their results and the earlier convection-tank data of Willis and Deardorff (1976, 1978, 1981) (hereafter WD76, WD78, WD81). Two studies also explored the concentration variance problem (Henn and Sykes and DdA06) with calculations of  $\sigma_c$ , the probability density function (PDF) of concentration, and other quantities along with comparisons to tank data. With the exception of Weil et al (2004), the investigators modeled dispersion by including a scalar diffusion equation in the LES model and adopted a diffusivity based on the subgrid-scale turbulent kinetic energy. In contrast, Weil et al. pursued a Lagrangian approach—an LPDM—similar to that of Lamb (1978) using LES velocity fields to drive the particle dispersion.

In this paper, we adopt the Weil et al (2004) model to construct an ensemble of dispersion realizations for sources in the CBL and address two key questions: 1) What is the predicted variability, i.e., the rms deviation, in dispersion properties given the turbulent wind field from an LES? and 2) How does the predicted variability in plume height, dispersion parameters, and concentrations compare with observations? In addition, we investigate two long-standing issues concerning surface source dispersion in the CBL: a) the applicability of similarity theory for the mean plume height (Yaglom, 1972), and b) the dependence of the mean surface concentration on downwind distance in very unstable conditions (e.g. Briggs, 1982; Nieuwstadt, 1980; Venkatram, 1992). The ensemble is built by modeling the particle trajectories and dispersion from each of 30 widely-separated sources at a given height in the CBL to create 30 “independent” realizations each approximating a 1/2-h averaging period. The source heights chosen match one in the WD76 experiment and two from the CONDORS (CONvective Diffusion Observed by Remote Sensors) field experiment (Briggs, 1993; Eberhard et al, 1988).

In the following, we give a brief background discussion on convective scaling of dispersion and the CONDORS field program (Section 2) while in Section 3, we present a short overview of the LES model and LPDM used in our dispersion modeling. Section 4 presents the main results on the mean and variability in the plume height, dispersion parameters, and concentration fields from sources in the CBL. This includes comparisons with data from convection tank experiments and field observations—the CONDORS and Prairie Grass experiments (Barad, 1958).

## 2 Background

### 2.1 Convective Scaling of Dispersion

Willis and Deardorff (1976) introduced convective scaling of dispersion to explain their laboratory dispersion results and relate them to full-scale observations. The scaling applies to a highly convective PBL in which the relevant turbulence length and velocity scales are the CBL depth  $z_i$  and the convective velocity scale:  $w_* = (g\overline{w\theta_0}z_i/T_a)^{1/3}$ , where  $g$  is the gravitational acceleration,  $\overline{w\theta_0}$  is the surface kinematic heat flux, and  $T_a$  is the ambient absolute temperature. The turbulence time scale is  $z_i/w_*$ , the eddy-turnover time. Due to the

strong convective mixing, the mean wind, potential temperature, and turbulence components exhibit little height variation within the “mixed layer” ( $0.1z_i \leq z < z_i$ ) and can be considered “well mixed” (e.g., Wyngaard, 1988). In addition, the mixed-layer turbulence components  $\sigma_u$ ,  $\sigma_v$ ,  $\sigma_w$  in the  $x$ ,  $y$ , and  $z$  directions can be taken as

$$\sigma_u, \sigma_v, \sigma_w \simeq 0.6w_* \quad (2)$$

based on observations (e.g., Hicks, 1985), where  $x$ ,  $y$ , and  $z$  are in the mean wind, crosswind, and vertical directions. The above description applies best when  $z_i/|L| > 50$  (Caughey, 1982), where  $L$  is the Obukhov length:  $L = -u_*^3 T_a / (kgw\theta_0)$ , where  $u_*$  is the friction velocity, and  $k$  is the von Kármán constant ( $= 0.4$ ).

Dispersion in the PBL is chiefly a function of time  $t$  after the release as is well known from statistical theory (Taylor, 1921). In convective scaling, Willis and Deardorff (1976) suggested that the time following the release be scaled as  $tw_*/z_i$  for an instantaneous source, and for a continuous source, they transformed this to a dimensionless distance  $X$ :

$$X = \frac{w_*x}{Uz_i}, \quad (3)$$

which is the ratio of the travel time  $x/U$  to the turnover time. Here,  $x$  is the distance downwind of the source, and  $U$  is the vertically-averaged wind speed in the CBL. They also proposed that the mean crosswind-integrated concentration (CWIC)  $C^y$  be put into the following dimensionless form

$$\frac{C^y U z_i}{Q} = f_1 \left( \frac{z}{z_i}, X, \frac{z_s}{z_i} \right), \quad (4)$$

where  $C^y = \int_{-\infty}^{\infty} C(x, y, z) dy$ ,  $Q$  is the source strength,  $z_s$  is the source height,  $y$  is the crosswind distance from the mean plume axis, and  $f_1$  is a dimensionless shape function. The dimensionless CWIC is the ratio of  $C^y$  to the uniformly-mixed scalar value  $Q/(Uz_i)$  far downstream.

For dispersion from a mixed-layer source, the rms dispersion parameters  $\sigma_y$  and  $\sigma_z$  in the crosswind and vertical directions can be predicted from statistical theory due to the approximate homogeneity of the turbulence in that layer (Hicks, 1985; Weil, 1988). For short times  $t < T_L$ , the predictions are  $\sigma_z = \sigma_w t$  and  $\sigma_y = \sigma_v t$ , where  $T_L$  is the Lagrangian integral time scale. With Eq. (2), the convective scaling versions of the expressions are  $\sigma_y/z_i \simeq \sigma_z/z_i \simeq 0.6X$ , where  $T_L$  is assumed  $\propto z_i/w_*$  (e.g., Briggs, 1993; Weil, 1988). Expressions of these and other forms are compared with the LPDM and observations in Section 4.

Laboratory experiments (WD76, WD78, WD81) and numerical simulations (Lamb, 1978, 1982) first showed the overall features of CBL dispersion and the importance of source height on the mean dispersion patterns. For a near-surface source ( $z_s/z_i = 0.067$ ), the average plume centerline ascended after a short distance  $X \simeq 0.5$ , whereas the centerline from an elevated source ( $z_s/z_i = 0.24$ ) descended until it reached the surface (Fig. 1). These behaviors were understood in terms of the release of material into updrafts and downdrafts (Lamb, 1982). For example, the centerline descent from the elevated source was caused by the greater areal coverage by downdrafts (60%) and the higher probability of material being released into them. In contrast, the Gaussian plume model predicted that the elevated plume centerline remained aloft and horizontal until a sufficient number of plume reflections occurred at the surface (Lamb, 1982).

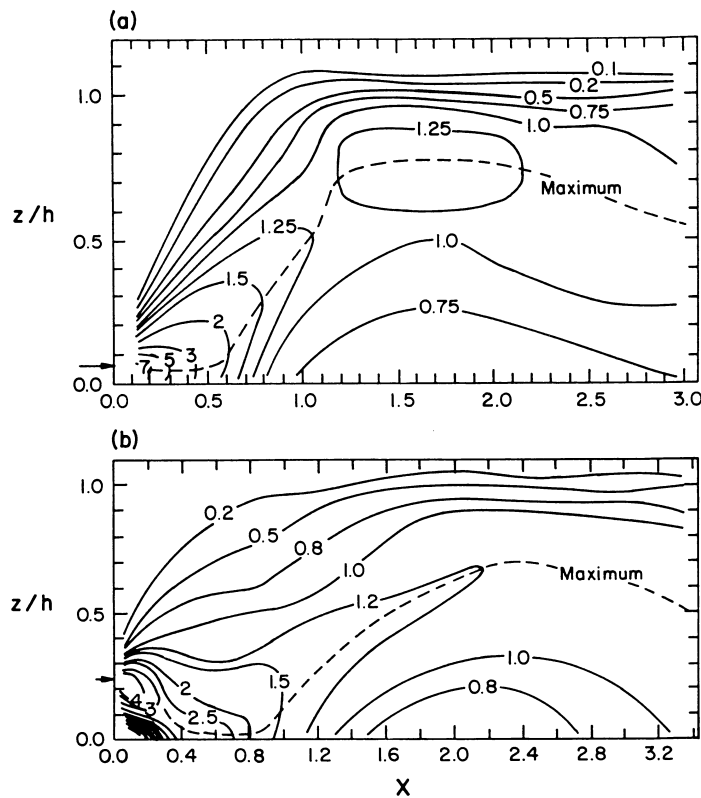


**Fig. 1** Convection tank results showing contours of dimensionless mean CWIC as a function of dimensionless height and downwind distance  $X$ , where  $h = z_i$ . Horizontal arrows denote source height: a)  $z_s/z_i = 0.067$ , adapted from Willis and Deardorff (1976); and b)  $z_s/z_i = 0.24$ , adapted from Willis and Deardorff (1978).

## 2.2 CONDORS Field Experiment

The CONDORS experiment was conducted during September 1982 and August-September 1983 near the 300-m Boulder Atmospheric Observatory (BAO) in Erie, Colorado, which is on the Colorado plains about 25 km east of the Rocky Mountain Foothills. The overall experimental objective was to determine the applicability of the non-Gaussian dispersion characteristics found in the convection tank experiments (WD76, WD78) and numerical simulations (Lamb, 1978, 1982) to full-scale plumes. The terrain within 15 km of the BAO was gently rolling with a surface cover consisting primarily of grasses, a few trees, and small scattered buildings; the estimated roughness height  $z_0$  was 3 cm for the CONDORS wind direction sector ( $50^\circ - 140^\circ$ ).

The desired meteorological conditions in the experiments were: 1) light winds and strong convection such that the CBL was dominated by convective turbulence throughout the layer (i.e.,  $z_i/|L| > 50$ ), and 2) a relatively low  $z_i$  such that a dimensionless source height  $z_s/z_i$  could be attained within the range of the Willis and Deardorff experiments:  $z_s/z_i = 0.24$  to 0.49. Archived tower data showed that these conditions could be satisfied often in the chosen August - September period during late morning to early afternoon. The

frequently-occurring meteorological scenario producing these conditions was easterly winds within the boundary layer (i.e., wind towards the Rocky Mountains) with westerly flow aloft, i.e., above  $z_i$ . The boundary layer winds were driven by surface heating of the mountain slopes, which generated an upslope flow. The range of conditions in the CONDORS data was:  $1.6 \text{ ms}^{-1} \leq U \leq 6.2 \text{ ms}^{-1}$ ,  $520 \text{ m} \leq z_i \leq 1600 \text{ m}$ ,  $1.38 \text{ ms}^{-1} \leq w_* \leq 2.1 \text{ ms}^{-1}$ ,  $0.84 \leq U/w_* \leq 4.4$ , and  $50^\circ \leq \phi_a \leq 140^\circ$ , where  $\phi_a$  is the wind direction (Briggs, 1993).

A specific aim of CONDORS was to obtain key dispersion characteristics—mean plume height, dispersion parameters  $\sigma_y$  and  $\sigma_z$ , the concentration field  $C(x, y, z)$ , and in particular the surface concentrations—as a function of distance and source height. The measurements were necessary for both surface and elevated sources since their behaviors were quite different (Fig. 1). The measurements required vertical profiles of scalars that could be obtained rapidly and repeatedly by ground-based remote sensors to determine 1/2-h to 1-h averages of dispersion properties. The scalar materials chosen were oil fog and aluminized chaff since they could be measured by lidar and Doppler radar, respectively. The BAO had an elevator for raising the oil and chaff disseminators to an elevated position and yielded  $z_s/z_i$  values ranging from 0.17 to 0.45 with most (five) near 0.33.

The lidar was positioned at a standoff distance about 4 km to the side of the plume and typically obtained 6  $y-z$  plume cross sections at different distances out to about 3.5 km downwind; each cross section was repeated a number of times to obtain averages over the sampling period (30 - 60 min, with an average of  $\simeq 38$  min). In contrast, the radar was located about 3.5 km upstream of the source and scanned a volume extending to about 4 km downwind of the source. The chaff settling velocity was about  $0.3 \text{ ms}^{-1}$  and not negligible. A simple model accounting for the settling showed that for a release height of  $0.33z_i$ , 24% of the material settled out after one eddy turnover time or for  $X = 1$  (Briggs, 1993).

The main conclusion from the CONDORS data analysis was that the observations supported the laboratory and numerical results of WD76, WD78 and Lamb (1978, 1982), respectively. Most of the elevated source plumes ( $z_s/z_i = 0.33$ ) were observed to have a downward tilting centerline that was similar to those from the laboratory data. In addition, the centerlines from the surface releases (primarily oil fog) lifted-off the surface to some extent at  $X \simeq 0.5$ , consistent with the tank experiments. Furthermore, the mean ground-level CWIC from the surface sources decreased with distance as  $X^{-3/2}$  in agreement with the laboratory and numerical data, and tended towards a minimum in the CWIC at  $X \simeq 1.5$  as found in the laboratory.

In addition, the mean plume heights from surface and elevated sources showed consistency with the laboratory data, but there was considerably more scatter in the observations. Indeed, a notable feature of all the measurements—plume height, dispersion parameters and surface CWICs—was the large data scatter. Briggs (1993) and Eberhard et al (1988) noted the usual fluctuations associated with light winds and strong convection, but they also pointed out the large variability due to the opposing winds in the CBL and aloft, i.e., above  $z_i$ . In many periods, there was strong shear in both wind speed and direction in the upper part of the CBL and above it; an example of this is shown in Fig. 4 of Wyngaard (1985).

The large scatter in the observations is the key focus of our LPDM-LES modeling and comparison with observations in Section 4.

### 3 Models

#### 3.1 Large-Eddy Simulations

The LES model used to provide the velocity fields for the LPDM was that of Moeng (1984) and Moeng and Sullivan (1994), the same one adopted by Weil et al (2004). The LES computes the wind, temperature, and pressure which are spatially filtered to define the resolved variables with eddy scales greater than the filter width  $\Delta$ , and the subfilter-scale (SFS) variables with scales less than  $\Delta$ . The filter width ( $\simeq 50$  m) is of the order of the numerical grid dimensions given below. For the LPDM, the LES variables that are stored in digital form are the three components of the resolved velocity, the temperature, and the SFS turbulent kinetic energy (TKE), which is used in parameterizing the SFS velocities. Details concerning the SFS stress tensor, turbulent eddy viscosity, dissipation rate, and other variables can be found in Moeng and Sullivan (1994). We use the same simulation and stored LES data as in Weil et al (2004).

The LESs were conducted for a CBL using a  $5 \text{ km} \times 5 \text{ km} \times 2 \text{ km}$  domain with  $96^3$  grid points and resulted in mesh spacings of  $\Delta x = \Delta y \simeq 52$  m and  $\Delta z \simeq 21$  m. Here,  $x$  is in the mean geostrophic wind direction,  $y$  is perpendicular to  $x$  in the horizontal plane, and  $z$  is the height above the ground. The surface heat flux ( $\overline{w\theta_o}$ ) was  $0.24 \text{ Kms}^{-1}$ , the average CBL depth  $z_i$  was 1000 m, and  $w_*$  was  $2 \text{ ms}^{-1}$  over the total simulation period of  $10z_i/w_*$ . Other variables in the LES were the surface roughness length  $z_0$  (0.16 m), the average friction velocity  $u_*$  ( $0.31 \text{ ms}^{-1}$ ), the vertically-averaged wind speed  $U$  over the CBL ( $3 \text{ ms}^{-1}$ ), and the Obukhov length  $L$  ( $-9.4$  m). The stability index  $-z_i/L$  characterizing the relative strengths of convective and shear-generated turbulence (Deardorff, 1972) was 106, which placed the CBL in the “highly convective” category. As a result, the mean wind profile was close to uniform over most of the CBL, and the velocity variances exhibited profiles typical of strong convection (see Weil et al, 2004).

#### 3.2 Lagrangian Particle Dispersion Model

In Lagrangian dispersion models, one tracks passive “particles” in a turbulent flow assuming that the particles behave as fluid elements and move with the local fluid velocity with molecular diffusion ignored. For a continuous source of constant strength  $Q$ , the mean concentration  $C$  can be found from

$$C(\mathbf{x}, t) = Q \int_{-\infty}^t p_1(\mathbf{x}, t; \mathbf{x}_{os}, t') dt' , \quad (5)$$

where  $p_1(\mathbf{x}, t; \mathbf{x}_{os}, t')$  is the position PDF for particles released at the source position  $\mathbf{x}_{os}$  at time  $t'$  being found at  $\mathbf{x}$  at time  $t$  (Lamb, 1978); a bold-faced symbol denotes a vector.  $p_1$  is computed from the numerically-calculated particle trajectories, and the particle position  $\mathbf{x}_p$  is found by integrating

$$\frac{d\mathbf{x}_p}{dt} = \mathbf{u}_L(\mathbf{x}_{os}, t) , \quad (6)$$

where  $\mathbf{u}_L$  is the Lagrangian velocity of a particle released at  $\mathbf{x}_{os}$ . This is termed a “one-particle” Lagrangian model wherein one follows thousands of particle trajectories to obtain the mean dispersion and concentration field (Wilson and Sawford, 1996).

In this work, we determine the Lagrangian velocity for particle tracking from the LES results using the Weil et al (2004) model and briefly describe the latter. We obtain  $\mathbf{u}_L$  as the sum of the LES resolved velocity component  $\mathbf{u}_r$  and a random SFS component  $\mathbf{u}_s$ :

$$\mathbf{u}_L(\mathbf{x}_{os}, t) = \mathbf{u}_r[\mathbf{x}_p(\mathbf{x}_{os}, t), t] + \mathbf{u}_s[\mathbf{x}_p(\mathbf{x}_{os}, t), t], \quad (7)$$

where  $\mathbf{u}_r$  and  $\mathbf{u}_s$  are found at the particle position at time  $t$ . This approach is similar to that of Lamb (1978) except for a more detailed stochastic SFS velocity formulation discussed below and a finer spatial resolution in the LES. The vertical grid length in Lamb's and our calculations was 50 m and 21 m, respectively.

In addition to the resolved velocity, the LES computes the unresolved or SFS TKE  $e_s$  at each grid point and time step. The random SFS velocity components  $u_{si}$  ( $i = 1 - 3$ ) are found from a stochastic differential equation in which the SFS TKE is assumed to be locally isotropic and Gaussian but inhomogeneous. The local isotropy assumption is consistent with most LES models at least in mid-PBL regions where the turbulence is well resolved (e.g., Moeng and Sullivan, 1994). For isotropic turbulence, the stress tensor is diagonal with components given by  $\sigma_s^2 = 2e_s/3$ . The increment of the SFS velocity  $u_{si}$  over the time step  $dt$  is based on the Lagrangian stochastic model of Thomson (1987) and is

$$du_{si} = -\frac{f_s C_0 \varepsilon}{2} \frac{u_{si}}{\sigma_s^2} dt + \frac{1}{2} \left( \frac{1}{\sigma_s^2} \frac{d\sigma_s^2}{dt} u_{si} + \frac{\partial \sigma_s^2}{\partial x_i} \right) dt + (f_s C_0 \varepsilon)^{1/2} d\xi_i, \quad (8)$$

where  $d\xi_i$  is a component of a Gaussian white noise,  $\varepsilon$  is the TKE dissipation rate, and  $C_0$  is an assumed universal constant, which we take as 3 (Weil et al, 2004). The  $f_s$  is a dimensionless coefficient ( $f_s \leq 1$ ) that represents the SFS fraction of the total TKE:

$$f_s = \frac{\langle \sigma_s^2 \rangle}{\langle \sigma_{av}^2 \rangle + \langle \sigma_s^2 \rangle}, \quad (9)$$

where  $\sigma_{av}^2 = (\sigma_{ru}^2 + \sigma_{rv}^2 + \sigma_{rw}^2)/3$ , the  $\sigma_{ru}^2$ ,  $\sigma_{rv}^2$ ,  $\sigma_{rw}^2$  are the resolved velocity variances in the three coordinate directions, and the angle brackets  $\langle \rangle$  denote an average over the horizontal plane.

The particle displacements for computing  $p_1$  and  $C^y$  (Eq. 5) are obtained by numerically integrating Eq. (8) to find  $u_{si}$ , substituting this and  $u_{ri}$  from the LES into Eq. (7), and inserting the resultant  $\mathbf{u}_L$  into Eq. (6) and integrating. This is the same approach as in Weil et al (2004).

### 3.3 Model Setup

In these simulations, passive particles were released from each of 30 sources at height  $z_s$  in a horizontal plane, where the sources had separations of 1 km ( $= z_i$ ) in the  $y$  direction and 1.5 km ( $= Uz_i/w_*$ ) in the  $x$  direction. The limited  $x - y$  domain (5 km  $\times$  5 km) could not accommodate all sources at once, and thus 20 sources were initiated at  $t' = 0$  with another 10 at  $t' = z_i/w_*$ . The turbulence field was horizontally homogeneous so that the turbulence statistics were the same at each source but due to the wide source separation, the time history and details of the velocity field at one source were different and independent of the others. From each source, 715 particles were released every 20 s ( $= 0.04z_i/w_*$ ) to simulate a continuous plume, and this was carried out for a 28-min period ( $\simeq 3.4z_i/w_*$ ). Thus, the total number of particles released was 60,775 per source and  $1.82 \times 10^6$  from all sources at each  $z_s$ .

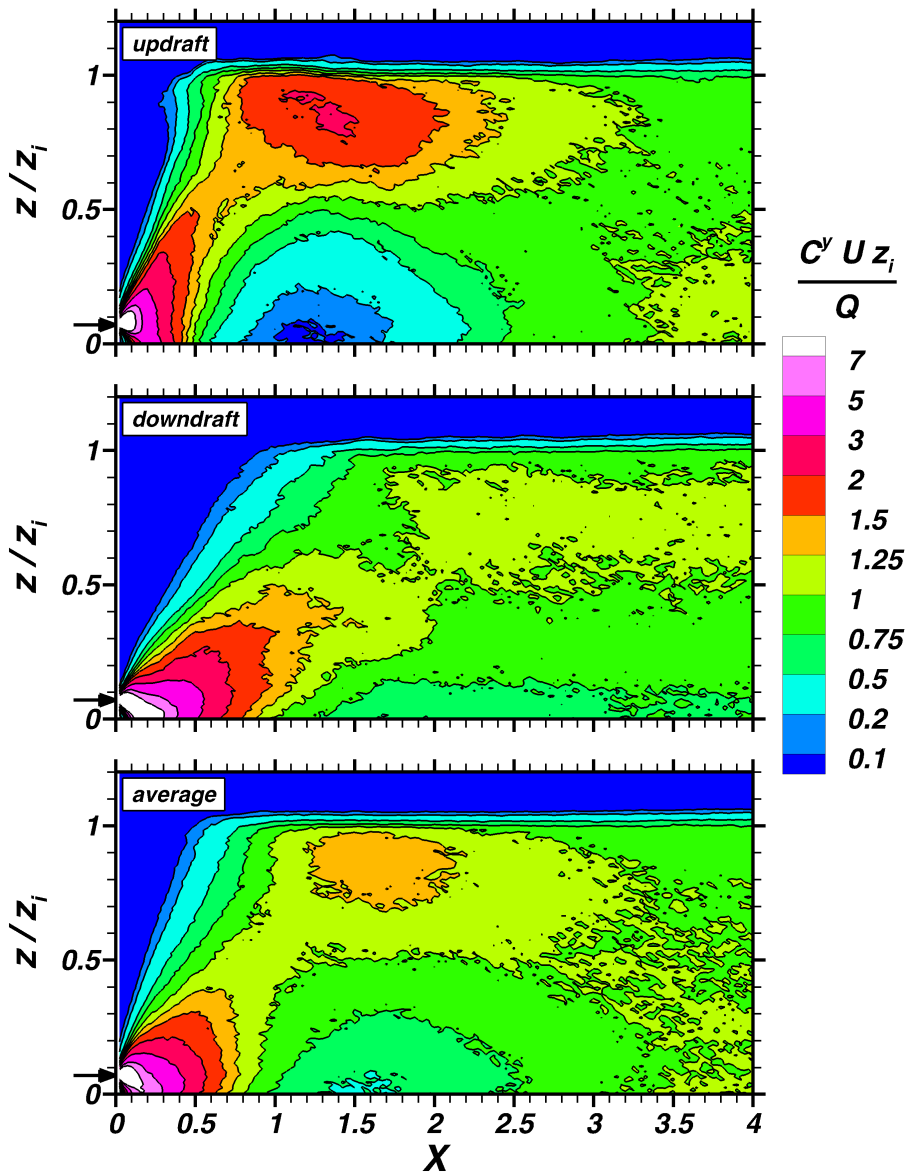


Fig. 2 LPDM crosswind-integrated concentration contours as a function of dimensionless height and downwind distance for: a) a strong updraft plume, b) a strong downdraft plume, and c) average over 30 realizations. Horizontal arrow marks the source height,  $z_s/z_i = 0.07$ ; averaging time of realizations is 28 min.

We performed simulations for three source heights: a surface source  $z_s/z_i = 0$ , a near-surface source  $z_s/z_i = 0.07$ , and an elevated source  $z_s/z_i = 0.32$ . The particle trajectory calculations were conducted with instantaneous velocity fields that were input sequentially from a large number (500) of LES data volumes. The volumes were stored at 10-s time intervals and each contained a  $96^3$  array of  $\mathbf{u}_r$  and  $e_s$ ; the total time period covered was  $10z_i/w_*$ . The interpolation of the LES velocity within a grid, the time step used in the particle trajectory calculations, and other details were the same as in Weil et al (2004).

In addition, we obtained the ensemble-mean CWIC from:

$$C^y(x, z) = \int_0^{t_f} p_1(x - x_{os}, z - z_{os}, t_d) dt_d, \quad (10)$$

where  $t_d = t - t'$ ,  $t_f = 1.5x_e/U$ , and  $x_e$  was the largest sampling distance of interest;  $p_1$  was found by averaging the particle position PDF's from the 30 realizations or sources (Weil et al, 2004). For each realization or source, Eq. (10) also was used but the  $p_1$  was calculated only for particles released from that source.

For a time-averaged plume, the spread is governed by both relative dispersion ( $\sigma_r$ ) about the meandering “instantaneous” centerline and plume meander within the averaging period  $T_{av}$ . In principle, the relative dispersion should be computed using a “two-particle” model (e.g., Thomson, 1990) while the within- $T_{av}$  meander is determined by resolved velocities of the large eddies (of scale  $\ell > \sigma_r$ ) in the LES. For the large  $T_{av}$  (28 min) results below (Section 4.1.2), this meander makes a significant contribution to the time-averaged dispersion. At dimensionless distances of say  $X > 0.3$  or 0.5, we believe that the one-particle model adopted here should be a good approximation to the dispersion and concentrations. Closer to the source, the one-particle model may overestimate the dispersion, resulting in an underestimate of the concentration peaks and rms concentration. This will be addressed in the future using a two-particle LPDM-LES, which is under development.

## 4 Results and Discussion

### 4.1 CWIC Fields and Spatial Moments

#### 4.1.1 Near-Surface Source: LPDM and Laboratory Data

An overview of the plume behavior for a near-surface source ( $z_s/z_i = 0.07$ ) is given by the modeled CWIC contour plots in Fig. 2. The dimensionless CWIC,  $C^y U z_i / Q$ , versus  $z/z_i$  and  $X$  is shown for three cases of the initial velocity at the source: a) a predominantly strong updraft, b) a predominantly strong downdraft, and c) the average CWIC over all 30 sources, where the main source differences are in the LES-resolved velocities. We assess the source updraft/downdraft strength based on the average plume height ( $\bar{z}_p$ ) at  $X = 1.3$  (Fig. 3) assuming that the larger and smaller  $\bar{z}_p$ 's are driven by the stronger updrafts and downdrafts, respectively; this  $X$  is the location of the minimum surface CWIC. The  $\bar{z}_p$  is given by

$$\bar{z}_p = \frac{\int_0^\infty z \bar{c}^y(x, z) dz}{\int_0^\infty \bar{c}^y(x, z) dz}, \quad (11)$$

where  $\bar{c}^y$  is the time-averaged CWIC in a realization. We refer to the initial velocity as a “predominantly” strong updraft or downdraft because that velocity structure probably occupied most but not the entire averaging period  $T_{av}$ , which is more than three times the eddy

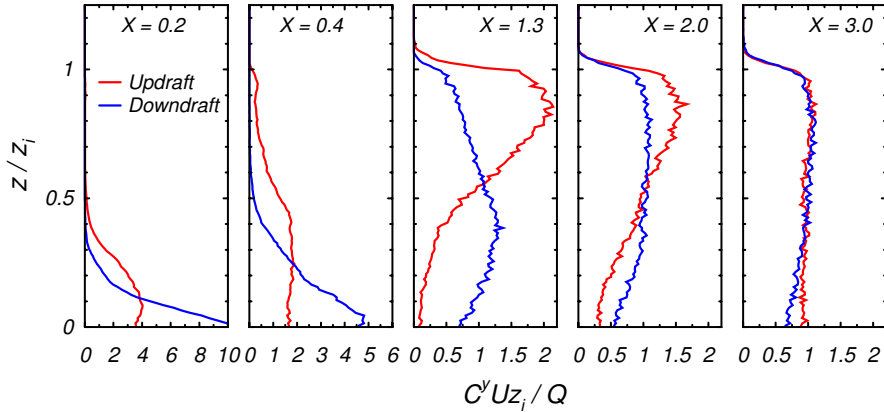


**Fig. 3** Vertical profiles of the dimensionless CWIC versus the dimensionless downwind distance  $X$  for the strong updraft and downdraft plumes in Fig. 2.

turnover time; i.e.,  $T_{av} \simeq 3.4z_i/w_*$ . Likewise, we refer to particle releases into updrafts as updraft plumes and similarly for downdrafts.

Figures 2a and 2b show three key differences between the strong updraft and downdraft plumes: 1) the updraft plume has a greater upward tilt of the plume axis near the source, 2) the updraft plume has much higher dimensionless CWICs ( $\simeq 2$  to 3) aloft, including an “anvil-like” region, than does the downdraft plume, and 3) the downdraft plume has much higher *surface* CWICs near the source as expected. The average CWIC field (Fig. 2c) lies between those for the updraft and downdraft plumes and agrees well with the convection tank results of WD76 (Fig. 1a), thus supporting these and other model results. The wide deviations between the updraft and downdraft plumes are further demonstrated by vertical profiles of the dimensionless CWIC versus  $X$  in Fig. 3. The profiles show the updraft/downdraft differences in the surface CWICs and the concentrations aloft, including the elevated maxima discussed above (see profiles at  $X = 1.3, 2$ ). The most distant profiles ( $X = 3$ ) are nearly well mixed except for the lowest region of the downdraft plume.

Figure 4 presents the dimensionless CWIC profiles versus  $X$  for all 30 realizations and shows that the ensemble-mean CWIC,  $C^y$  (red line), agrees well with the WD76 data; i.e., all data are within the scatter of the modeled realizations. The figure also demonstrates the evolution of the plume from a small compact distribution at short range ( $X = 0.12$ ) where the maximum CWIC is at the surface to one with an elevated maximum at  $X = 1.55$ ; the CWIC evolves to an approximately well-mixed profile by  $X \simeq 3$ . The elevated maximum is a unique feature of a highly convective PBL and results from the vertical gradient of  $\sigma_w$  in combination with a large  $T_L$  ( $\simeq z_i/w_*$ ) that lead to a mean upward “drift” velocity (Sawford and Guest, 1987; Weil, 1990). From a phenomenological view, Lamb (1982) reasons that material released into the base of an updraft begins rising almost immediately, whereas that released into a downdraft remains near the ground and moves horizontally. Once a significant amount of material is swept out of downdrafts into neighboring updrafts, the plume centerline begins rising and “lifts-off” the surface.

The CWIC variability in Fig. 4 is greatest at the surface and close to the source ( $X \leq 0.5$ ), but at  $X = 1.55$ , it is as large in the upper part of the CBL as at the surface. The latter is due to the superposition of high- and low-CWICs from the updraft- and downdraft-dominated

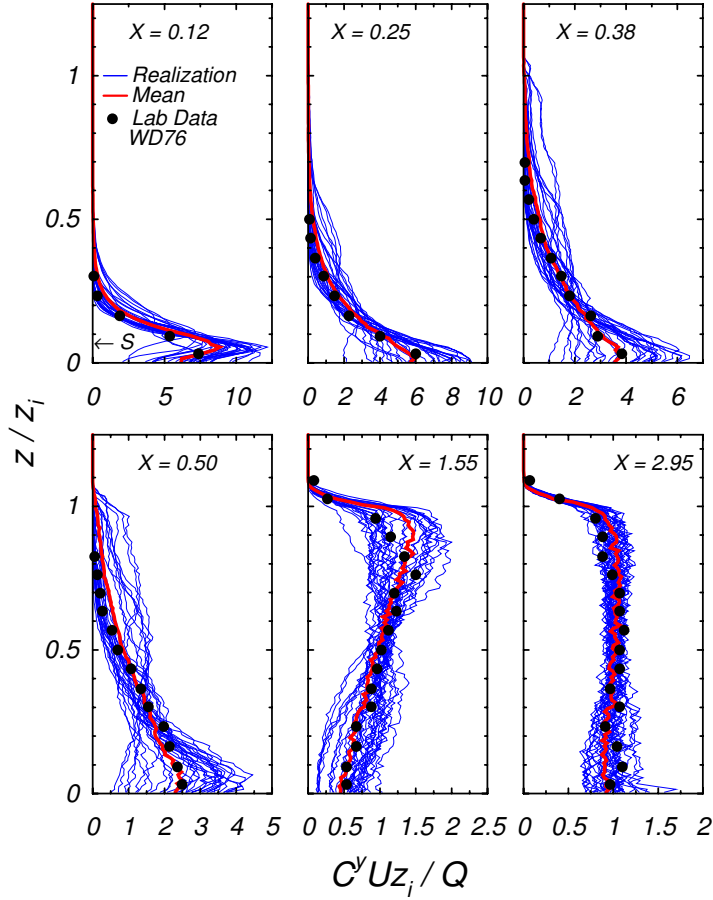


**Fig. 4** Vertical profiles of the dimensionless CWIC versus the dimensionless downwind distance  $X$  for 30 LPDM realizations and the ensemble-mean CWIC; also shown are the Willis and Deardorff (1976) tank data of the mean CWIC. Source height is  $z_s/z_i = 0.07$  and denoted by  $S$  in the  $X = 0.12$  panel.

sources, respectively. Relative to the mean CWIC, updrafts lead to negative CWIC perturbations at the surface and positive perturbations aloft, whereas the opposite is true for downdrafts; see also Fig. 3. The variability decreases as the plume becomes vertically homogenized and approaches a well-mixed state ( $X \simeq 3$ ).

Figure 5 presents the average plume height  $\bar{z}_p$  from each of the 30 realizations and the ensemble-mean value  $\langle \bar{z}_p \rangle$ . It shows that the  $\langle \bar{z}_p \rangle$  (red line) agrees well with the WD76 data giving further credibility to the LPDM and that about 40% of the individual trajectories lie above  $\langle \bar{z}_p \rangle$  with the remainder below it. This is consistent with the vertical velocity ( $w$ ) PDF in the CBL, where the horizontal area coverage by updrafts and downdrafts is about 40% and 60%, respectively (Lamb, 1982). The difference in the areal coverage leads to a positive skewness,  $S_w = \bar{w}^3 / \sigma_w^3$ , which averages about 0.6 - 0.8 in a highly convective PBL (e.g., Wyngaard, 1985, 1988; Moeng and Sullivan, 1994).

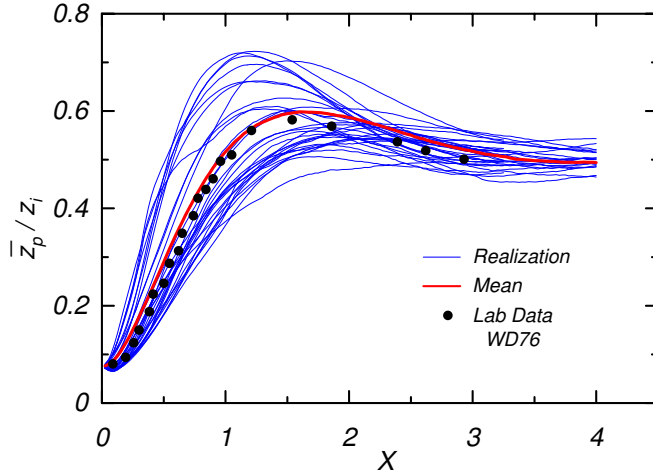


**Fig. 5** LPDM realizations and ensemble mean of the average plume height versus the dimensionless distance  $X$  with comparisons to the Willis and Deardorff (1976) tank data of the mean height; source height is  $z_s/z_i = 0.07$ .

#### 4.1.2 Surface and Elevated Sources: LPDM and CONDORS Observations

Here, we compare the LPDM realizations, mean value, and rms deviations in dispersion properties—plume height, dispersion parameters ( $\sigma_y$ ,  $\sigma_z$ ), and surface CWICs—with observations from the CONDORS experiment. The two CONDORS cases selected are those with multiple releases from a given height: a surface source and an elevated source ( $z_s/z_i = 0.32$ ) with 10 and 5 repetitions, respectively. A key assumption is that for a given source height the scaled or dimensionless properties as a function of  $X$  are independent of stability since  $z_i/|L| > 50$ . Thus, any variability in scaled properties is assumed due to the differences and randomness in the velocity field at the various sources, i.e., the differences in the realizations.

For the surface source, the CWIC fields (not shown) are similar to results for the near-surface source presented in Fig. 2. However, in the case of the elevated source, the CWIC fields (Fig. 6) exhibit more distinct upwardly- and downwardly-directed plumes for the strong updraft and downdraft cases (Figs. 6a, 6b) by comparison to Fig. 2. In addition, the updraft plume concentrations are not as high near the CBL top as those in Fig. 2a, which is due to the greater turbulence levels and initial dispersion for the elevated release than the near-surface source; i.e.,  $\sigma_w/w_* \simeq 0.65$  and  $0.42$  at  $z_s/z_i = 0.32$  and  $0.07$ , respectively. Moreover, Fig. 6 shows that the updraft and downdraft plumes exhibit differences in their short-range *surface* CWICs that are similar to or possibly larger than those in Fig. 2. Finally, the average CWIC field for the elevated source (Fig. 6c) is qualitatively similar to that from the WD78 convection tank experiments for a somewhat lower release height ( $z_s/z_i = 0.24$ ; Fig. 1b).

In Fig. 7, we compare the LPDM realizations, ensemble mean, and rms deviation of the plume height with CONDORS observations for the surface and elevated sources. In both cases, the realizations and rms spread (mean  $\bar{z}_p/z_i \pm$  rms deviation  $\sigma$  in  $\bar{z}_p/z_i$ ) overlap well with the measurements and generally reproduce the trend of the data scatterband with

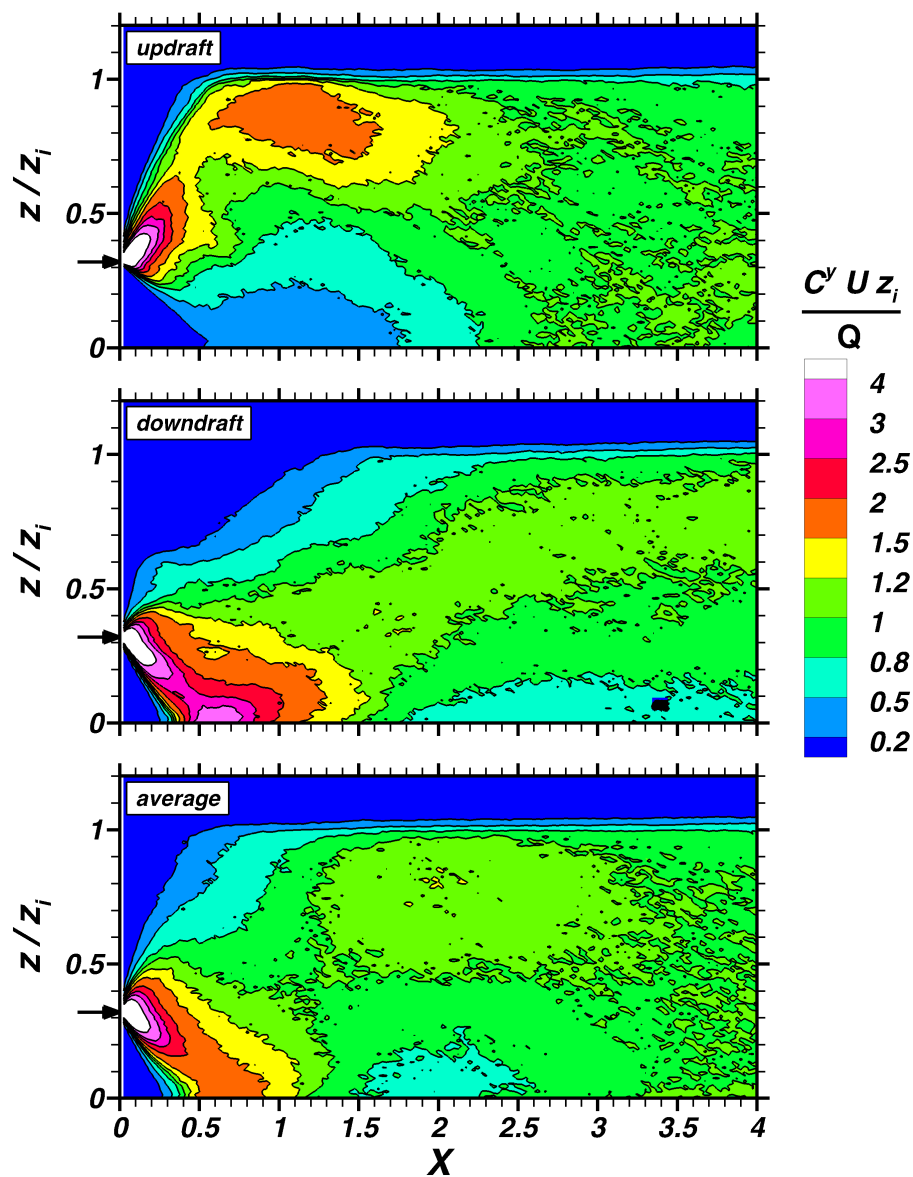


**Fig. 6** LPDM CWIC contours as a function of dimensionless height and downwind distance for: a) a strong updraft plume, b) a strong downdraft plume, and c) average over 30 realizations. Horizontal arrow denotes the source height,  $z_s/z_i = 0.32$ ; averaging time of realizations is 28 min.

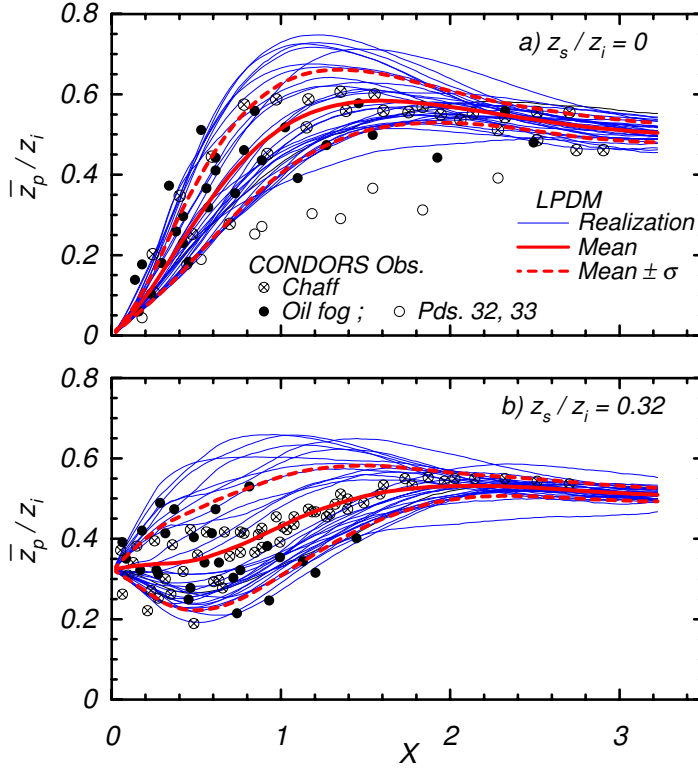


**Fig. 7** Dimensionless plume height as a function of dimensionless distance for LPDM realizations and ensemble-mean value with comparison to CONDORS data. In this and following figures, the red solid line is the ensemble mean of the variable over all 30 realizations, and the red dashed lines are the mean  $\pm \sigma$ , where  $\sigma$  is the rms deviation of the variable over the 30 realizations.

$X$ . This is true for both the oil and chaff data with the exception of two “outlier” periods for the surface release [Periods (Pds) 32, 33; open circles]. Briggs (1993) classified the outliers as cases of “squashed plumes” caused by a persistent mean downdraft at or near the source since in both periods, the mean vertical velocity  $\bar{w}$  was negative on the upper levels (100 m - 300 m) of the BAO:  $\bar{w} = -0.33 \text{ ms}^{-1}$  and  $-0.69 \text{ ms}^{-1}$  over the 1/2- to 1-h averaging periods. Some potential causes of this behavior are: 1) large persistent eddies or possibly rotors formed by downslope winds over the Rocky Mountains and their interaction with the CBL turbulence, 2) strong wind speed shear at the PBL top (Section 2.2) with the possible generation of large eddies interacting with the CBL turbulence, and 3) horizontal inhomogeneities in surface heat flux due to variations in land use, irrigation, and soil drying conditions as noted by Briggs (1993).

Figure 8 presents the vertical dispersion for both sources and shows that for  $X < 0.7$ , the LPDM variability in  $\sigma_z$  as given by the range of the realizations and rms deviation agree well with the observed scatter. The  $\sigma_z$  about the average height is obtained from

$$\sigma_z^2 = \frac{\int_0^\infty (z - \bar{z}_p)^2 \bar{c}^y(x, z) dz}{\int_0^\infty \bar{c}^y(x, z) dz}. \quad (12)$$

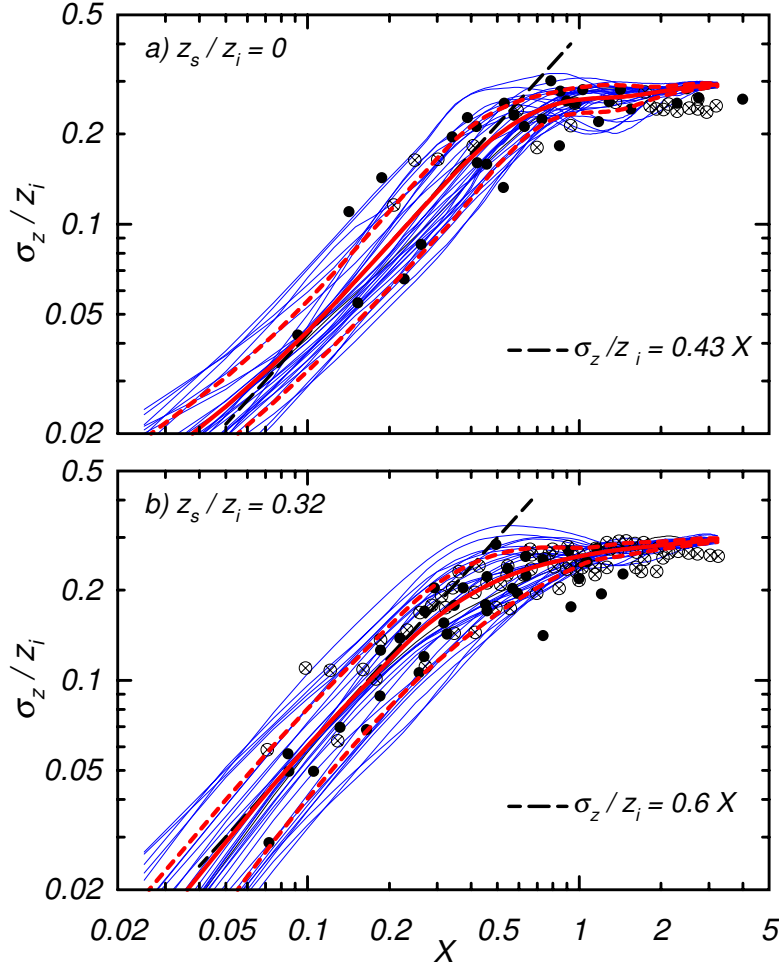


**Fig. 8** LPDM realizations and ensemble mean of dimensionless vertical dispersion versus dimensionless distance and comparison with CONDORS data. Key to LPDM lines and CONDORS data same as in Fig. 7.

At small  $X$  ( $< 0.4$ ), the mean dispersion (solid red line) is approximated well by the short-time prediction of statistical theory in the dimensionless form:  $\sigma_z/z_i = a_z X$ , where  $a_z = \sigma_w/w_*$ . This is shown by the dashed lines with  $a_z = 0.43$  and  $0.6$  for the surface and elevated sources, respectively. The  $a_z = 0.6$  approximates the  $\sigma_w/w_*$  for the elevated source ( $\sigma_w/w_* = 0.65$ ) and is consistent with turbulence measurements (e.g., Caughey, 1982; Hicks, 1985), and  $a_z = 0.43$  could be interpreted as an “effective  $\sigma_w/w_*$ ” for the surface source. The LPDM mean asymptotes to  $\sigma_z/z_i = 0.29$  ( $= 1/\sqrt{12}$ ) at large  $X$  ( $\simeq 3$ ), corresponding to a vertically well-mixed distribution about the mean height,  $0.5z_i$  (e.g., Briggs, 1993). For  $X > 1$ , more of the observations fall below this asymptote and tend towards  $\sigma_z/z_i \simeq 0.26$ . For the surface source, the lower  $\sigma_z$  for the oil data might be explained by the “squashed-plume” cases, and for both sources, the lower chaff dispersion may be partially due to gravitational settling.

Figure 9 shows LPDM results of the lateral dispersion,  $\sigma_y/z_i$  versus  $X$ , along with data from the CONDORS and Prairie Grass (PGr) experiments where the PGr data is only available for the surface release (Fig. 9a); the  $\sigma_y$  is obtained from  $y$  moments using an expression similar to Eq. (12). For the surface source, the model and data are in good overall agreement with most of the observations falling within the modeled rms deviation (red dashed lines) of the realizations. For this source and  $X \ll 1$ , the results tend to a linear variation of  $\sigma_y/z_i$  with  $X$  as expected based on statistical theory and the homogeneity of the horizontal turbulence in the CBL (e.g. Weil, 1988). However, the mean short-time or distance limit— $\sigma_y/z_i = X$  (solid red line)—exceeds the usual prediction  $\sigma_y/z_i = 0.6X$  given in Section 2.1. This is caused by the enhanced  $\sigma_v$  and reduced mean wind  $\bar{u}(z)$  near the surface as found in the LES (Fig. 1; Weil et al, 2004) and observations (Fig. 3; Briggs, 1993).

At large times or distances ( $t \gg T_L$  or  $X \gg 1$ ), the LPDM mean prediction tends towards a  $\sigma_y \propto t^{1/2}$  or  $X^{1/2}$  dependence as given by statistical theory (Taylor, 1921) since the LES lateral turbulence is horizontally homogeneous. The dimensionless form of this prediction is  $\sigma_y/z_i = [2(\sigma_v/w_*)^2 T_{Ly}^* X]^{1/2}$  (e.g., Weil, 1988) and from the LPDM results, we infer a dimensionless time scale  $T_{Ly}^* = T_{Ly} w_*/z_i \simeq 0.6$ . In Fig. 9a, we also show Briggs (1993) semi-empirical expression (green line), which agrees with the data and the LPDM for  $X \leq 1$ , but for  $X > 1$  the two curves diverge. There are insufficient observations for  $X > 1$  to determine the more appropriate prediction.

For the elevated source (Fig. 9b), the LPDM underestimates both the mean and variability of the observed lateral dispersion. An approximate fit to the LPDM short-range limit is  $\sigma_y/z_i = a_y X$  with  $a_y = 0.45$ , whereas the observed average has an  $a_y$  closer to 0.6; see dashed line. The underestimated  $\sigma_y$  is due to the small  $\sigma_v$  predicted by the LES which is  $\sigma_v \simeq 0.46w_*$  at source height (Weil et al, 2004) and is consistent with the  $\sigma_v$  inferred from the LPDM mean  $\sigma_y$ . A lower-than-observed  $v$  variance can be expected for LES of weak-wind CBLs that do not include a mesoscale forcing or mesoscale-generated turbulence (Nieuwstadt et al, 1993). The model results in Fig. 9b also tend towards a  $\sigma_y \propto t^{1/2}$  or  $X^{1/2}$  behavior at large  $X$  as expected for the horizontally homogeneous turbulence in the LES, but the data show no trend towards an  $X^{1/2}$  dependence. There are two possible causes for this and the larger-than-1/2 exponent on  $X$ : 1) a poorly-defined and growing turbulence lengthscale due to horizontal inhomogeneities and mesoscale turbulence, and 2) wind direction shear in the upper part of the CBL as observed during CONDORS (Briggs, 1993; Eberhard et al, 1988). The shear-induced dispersion  $\sigma_{ys}$  is given by  $\sigma_{ys} \propto (\partial V/\partial z)\sigma_z t$  (e.g., Smith, 1965; Venkatram, 1988a), where  $V$  is the mean crosswind velocity. With  $\sigma_z \simeq$  constant for a well-mixed plume, this leads to  $\sigma_{ys} \propto t$  or  $x$ , and could explain some of the observations in Fig. 9b for  $X > 1$ .

One of the most important variables needed in dispersion applications is the ground-level concentration. For a surface release, surface layer similarity (SLS) is a proven approach for estimating the surface concentration and CWIC over a broad range of stability and thus is a good standard for comparison (Horst, 1979; van Ulden, 1978). The theory is based on the Monin-Obukhov (MO) similarity profiles of mean wind, turbulence, and eddy diffusivity in the atmospheric surface layer. The ensemble-mean CWIC at the surface is dependent on the mean plume height through

$$C^y(x, y) = \frac{AQ}{U_p \langle \bar{z}_p \rangle}, \quad (13)$$

where  $U_p(x)$  is the average wind speed over the plume depth at  $x$ , and  $A$  is a parameter dependent on the shape of the vertical concentration profile. However, SLS theory ignores the capping inversion and the different turbulence conditions in the mixed layer ( $0.1z_i \leq z <$

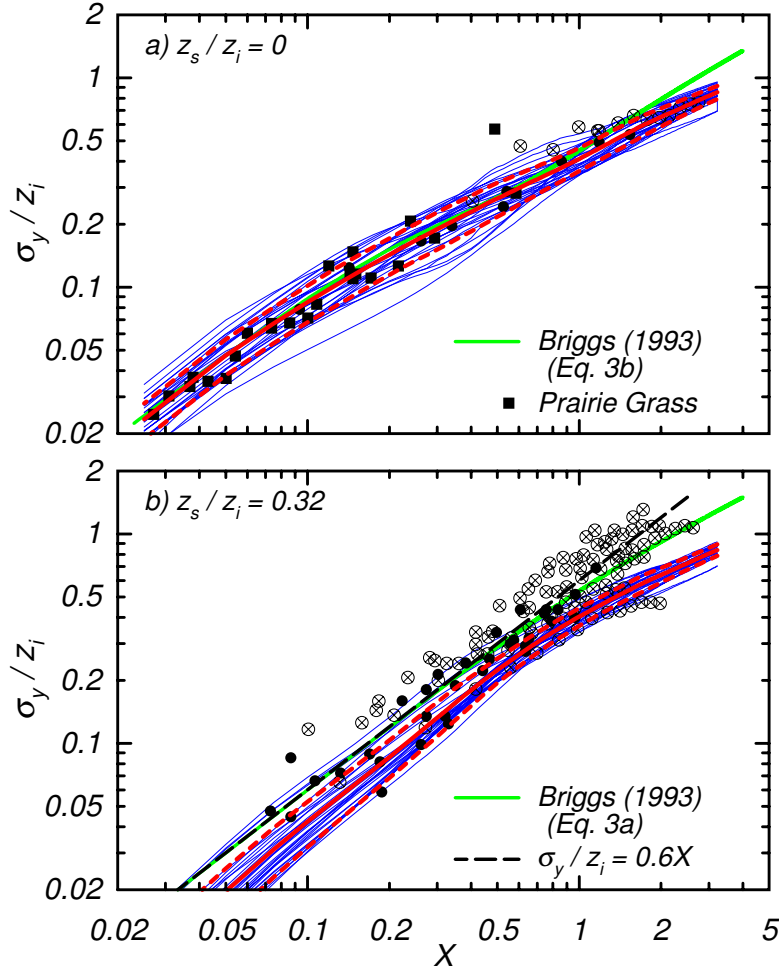


**Fig. 9** LPDM realizations and ensemble-mean of dimensionless crosswind dispersion versus dimensionless distance and comparison with CONDORS data; key to LPDM lines and CONDORS data same as in Fig. 7. In a), Briggs (1993) curve (his Eq. 3b) is:  $\sigma_z/z_i = 0.6X/(1+X^2)^{1/6} + (0.4X - X^2)/(1+6X^2)$ , and in b) same as in a) but without second term.

$z_i$ ) and surface layer ( $z < 0.1z_i$ ). Thus, its applicability is restricted to short distances before the mixed-layer effects are felt, say  $X < 0.5$ .

Figure 10 presents the dimensionless CWIC at the surface as a function of  $X$  for the surface source and shows that the LPDM mean is in fair agreement with SLS theory except close to the source ( $X \leq 0.1$ ), where the model sampling grid ( $\Delta X = 0.025$ ) is probably too coarse to resolve the  $C^y$  longitudinal gradient. For  $X > 0.3$ , most of the observations fall within the predicted rms error band, except for the “squashed plume” cases, and almost all of the data fall within the range of the LPDM realizations. This is encouraging and suggests that the turbulence variability—in the LES resolved-velocity field—is the principal cause of the CWIC variability. The observations falling along the lower bound of the realizations are

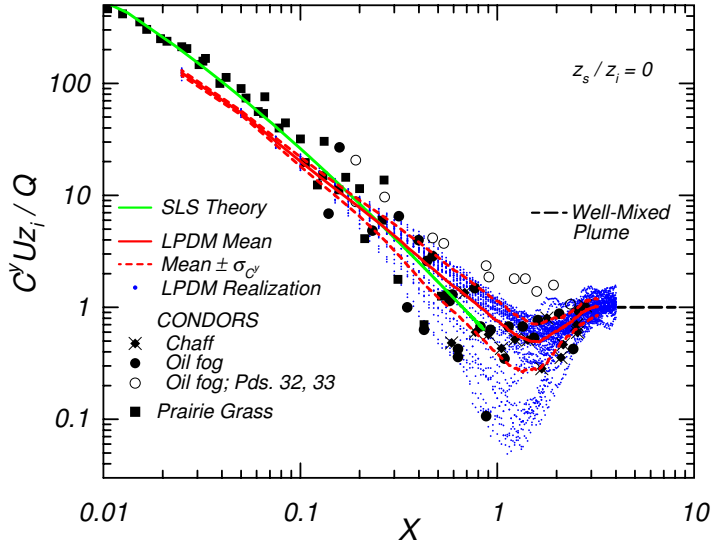


**Fig. 10** Dimensionless CWIC at the surface as a function of  $X$  for a surface source showing LPDM realizations and ensemble mean with comparisons to surface layer similarity theory, CONDORS observations, and Prairie Grass data.

caused by strong updraft plumes as discussed below (Section 4.2.3). The modeled mean also tends towards the correct CWIC large- $X$  asymptote of a well-mixed plume:  $C^y U z_i / Q = 1$  at  $X \simeq 3$  or 4. The main exceptions to the above results are the CONDORS data for Pds 32, 33—the “squashed plume” cases, which had unusually low mean plume heights (Fig. 7a) and thus would be expected to have unusually high surface CWICs as found. This follows from applying the SLS result (Eq. 13) to the individual realizations,  $\bar{c}^y \propto Q / (\bar{u}_p \bar{z}_p)$ , where  $\bar{u}_p(x)$  is the average plume transport speed in the realization.

For  $0.1 \leq X \leq 0.3$  (Fig. 10), the computed variability underestimates the observed scatter for several possible reasons. First, the one-particle model used results in a larger spread and lower concentrations than would a 2-particle LPDM at these distances (Section 3.3). Second, the vertical resolution of the particle sampling grid ( $\Delta z / z_i = 0.01$ ) may be too coarse to sample the plume adequately in this region. Third, the LES is run for only one case ( $U = 3 \text{ ms}^{-1}$ ,  $z_i = 1000 \text{ m}$ ,  $w_* = 2 \text{ ms}^{-1}$ , etc.), whereas the field data comprise a range of conditions (Section 2.2) which may result in more scatter. Finally, there is uncertainty due to experimental error in the observed  $U$ ,  $z_i$ , heat flux, and other variables, and 30 may be an insufficient number of realizations.

Figure 11 shows the LPDM surface  $C^y$  results and CONDORS observations for the elevated source,  $z_s / z_i = 0.32$ , and the expected increase of the dimensionless mean CWIC to a maximum value ( $\simeq 2.1$ ) at a dimensionless distance  $X \simeq 0.6$ . As can be seen, the predictions are in good agreement with the observations with all but two of the data points falling within the range of the LPDM realizations and most of them lying within the rms deviation of the mean. The exceptional cases are chaff data and might be attributed to the settling velocity since they occur on the upstream side of the predicted CWIC field. The mean LPDM results are similar to those of WD78 and Lamb (1982) for a source at  $z_s / z_i = 0.24$ . For  $X < 0.4$ , the modeled variability as measured by the ratio of maximum/minimum CWIC ranges over

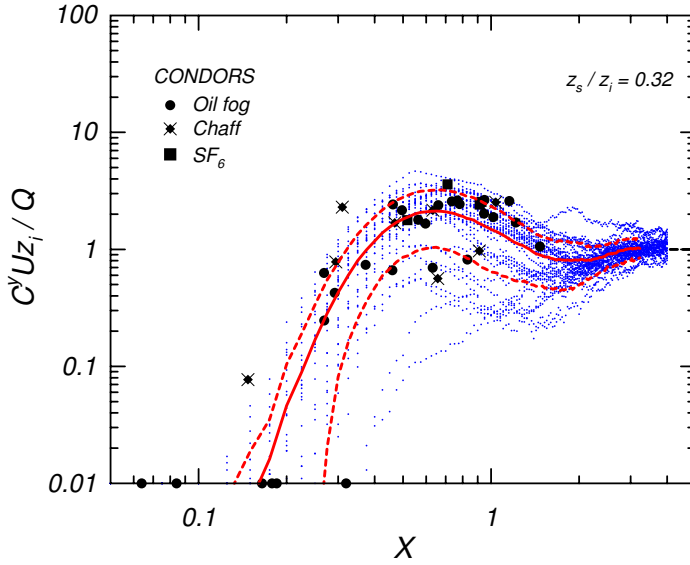


**Fig. 11** Dimensionless CWIC at the surface as a function of  $X$  for an elevated source ( $z_s/z_i = 0.32$ ) showing LPDM realizations and ensemble mean with comparison to CONDORS data. Key to LPDM lines same as in Fig. 10.

two orders of magnitude and is far greater than that for the surface source at this range (Fig. 10). Such variability is due to the meandering of the small elevated plume by the large CBL eddies. At greater distances,  $1 < X < 3$ , the modeled CWIC variability is lower by about a factor of 10 due to the reduction in the plume meander ( $\sigma_{zm}$ ; Fig. 12b) and the approach of the CWIC to a vertically well-mixed distribution.

The large scatter in Fig. 11 helps to explain the low correlation usually found between modeled and observed surface concentrations from tall stack releases in the CBL (e.g., Hanna and Paine, 1989; Venkatram, 1988b; Weil et al, 1992). The modeled values are estimates of the ensemble-mean concentration whereas the observations are individual realizations, which exhibit much scatter as shown in Fig. 11.

## 4.2 Further Analysis and Discussion

### 4.2.1 Rms Meander and CWIC Fluctuation Intensity

The rms meander of a small wandering plume is an important and necessary variable in “meandering plume” dispersion models (e.g., Gifford, 1959; Luhar et al, 2000; Sykes, 1988). The meander can cause infrequent “spikes” of high concentration at a monitor, which may result in low mean concentrations but large rms values,  $\sigma_c$ 's. Here, we analyze the rms meander in the crosswind and vertical directions,  $\sigma_{ym}$  and  $\sigma_{zm}$ , and the surface-CWIC fluctuation intensity,  $\sigma_{C^y}/C^y$ , from the LPDM simulations. One of our purposes is to assess the effect of time-averaging on the meander.

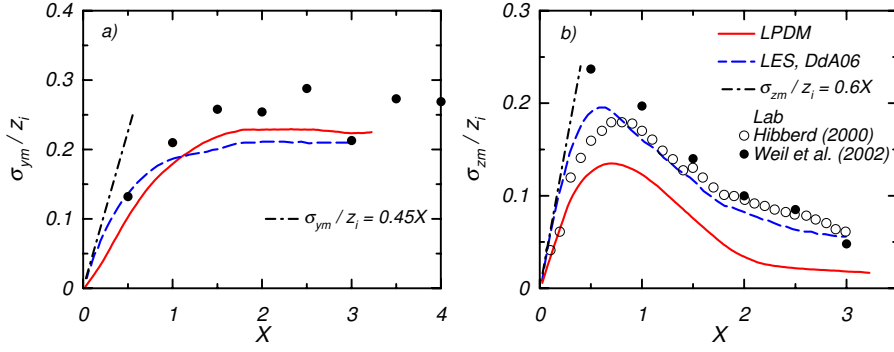


**Fig. 12** Dimensionless rms plume meander as a function of  $X$  for a) crosswind and b) vertical dispersion components. LPDM for  $z_s/z_i = 0.32$  and 28-min average; DdA06 LES and Hibberd (2000) tank data for  $z_s/z_i = 0.25$  and near-instantaneous plume; and Weil et al (2002) tank data for effective source height of  $0.3z_i - 0.4z_i$  and near-instantaneous plume. LPDM  $\sigma_{ym}$  and  $\sigma_{zm}$  are the rms deviations of plume lateral position  $\bar{y}_p$  and height  $\bar{z}_p$  for a 28-min time-average about their ensemble-mean values,  $\langle \bar{y}_p \rangle$  and  $\langle \bar{z}_p \rangle$ , over the 30 realizations.

The  $\sigma_{ym}$  is given by

$$\sigma_{ym} = \left( \frac{1}{M} \sum_{j=1}^M (\bar{y}_{pj} - \langle \bar{y}_p \rangle)^2 \right)^{1/2} \quad (14)$$

where  $\bar{y}_{pj}$  is the mean crosswind displacement of the  $j$ th realization,  $\langle \bar{y}_p \rangle$  is the ensemble-mean value, and  $M$  is the number of realizations; the  $\sigma_{zm}$  is found similarly. In homogeneous turbulence, Csanady (1973) argues that the meander should behave as

$$\sigma_{ym} = \sigma_v t \quad t \ll T_{Ly} \quad (15a)$$

$$\frac{d\sigma_{ym}^2}{dt} = 0 \quad t \gg T_{Ly}, \quad (15b)$$

where  $T_{Ly}$  is the Lagrangian time scale for the lateral turbulence. Thus,  $\sigma_{ym}$  should tend to a constant at large times or distances.

Figure 12a shows the crosswind meander for an elevated source and includes results from the LPDM-LES for  $z_s/z_i = 0.32$ , the DdA06 LES for  $z_s/z_i = 0.25$ , and the convection tank data of Weil et al (2002). Although the tank data are for a lower release ( $z_s/z_i = 0.15$ ), the source exit momentum leads to an “effective” source height of  $\simeq 0.3z_i - 0.4z_i$ , which is close to the other  $z_s$  values. The results from the LES and experiments are in approximate agreement and support the expected trend of  $\sigma_{ym}/z_i$  with  $X$  from Csanady’s theory—e.g., the constant  $\sigma_{ym}$  at large  $X$ . The laboratory data and DdA06 results apply to a near-instantaneous plume and thus should exceed the  $\sigma_{ym}$  of the time-averaged plume, which is true for the tank data. However, for  $X > 1$ , the DdA06 result is somewhat lower than expected. Nevertheless, the overall consistency with Csanady’s theory is good for this case of homogeneous turbulence with a well-defined length scale ( $z_i$ ). The estimation of the meander for the “outdoor” CBL is more problematic because of the ill-defined lateral lengthscale due to horizontal inhomogeneities and mesoscale turbulence effects.

Within the mixed layer,, the turbulence can be approximated as homogeneous, and thus the short-time meander prediction of Csanady (1973) should apply to the vertical component:  $\sigma_{zm} = \sigma_w t$  for  $t \ll T_{Lz}$ , where  $T_{Lz}$  is the Lagrangian time scale for the  $w$  component.

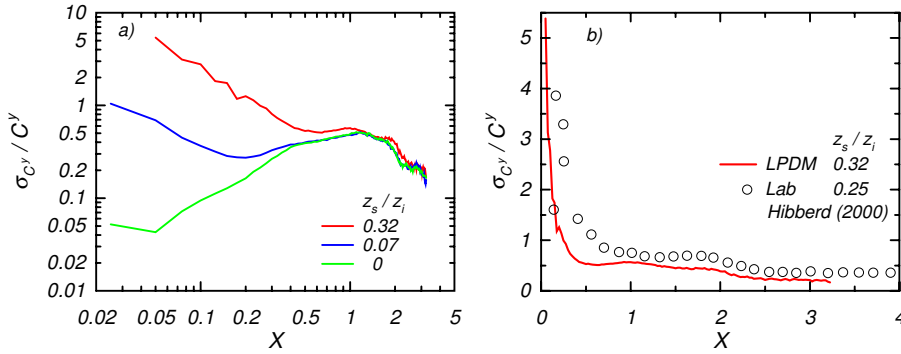
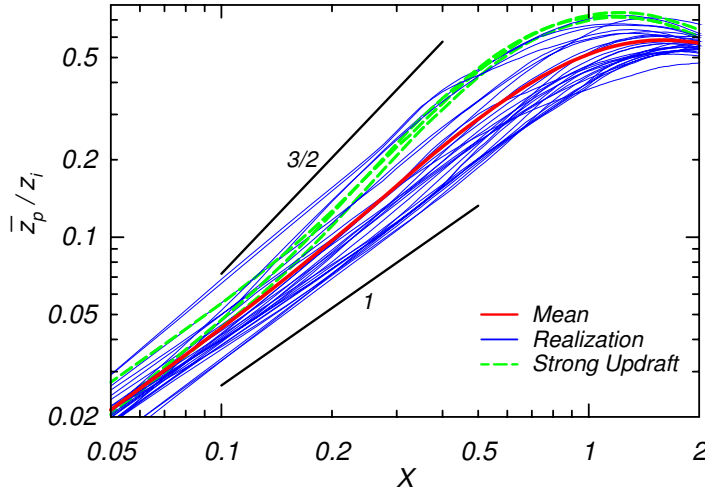


**Fig. 13** LPDM CWIC fluctuation intensity at the surface versus dimensionless distance for: a) three source heights, and b) elevated source with comparison to Hibberd (2000) data. LPDM  $\sigma_{C^y}$  is the rms deviation of the time-averaged CWIC  $\bar{c}^y$  about the ensemble-mean value  $C^y$  over the 30 realizations.

However, for a vertically-bounded environment such as the CBL, the meander must tend to a small value and eventually to zero as  $t \gg T_{Lz}$  or  $X \gg 1$  due to plume interaction with the boundaries. Thus, the expected shape of  $\sigma_{zm}/z_i$  with  $X$  should be linear for  $X \ll 1$ , zero at large  $X$ , with a local maximum at some intermediate  $X$  (Nieuwstadt, 1992).

Figure 12b presents the  $\sigma_{zm}/z_i$  from the LPDM-LES for the elevated source along with the DdA06 results and convection tank data (Hibberd, 2000; Weil et al, 2002). The data and DdA06 predictions, all for a near-instantaneous plume, exhibit a general consistency with one another and show the expected shape of  $\sigma_{zm}/z_i$  versus  $X$  including a linear spread for  $X \ll 1$ . With respect to source height, the best overlap between the DdA06 and LPDM results is with the elevated release,  $z_s/z_i = 0.32$ . In this case, the LPDM curve has the same shape as that of DdA06 but is shifted downwards by about 35% over the range  $0 < X \leq 1.5$ . For larger  $X$ , the  $\sigma_{zm}$  decreases at an even faster rate, which we believe is due to the greater spread ( $\sigma_z$ ) of the time-averaged plume; i.e., the wider plume interacts with the boundaries sooner in  $X$  to limit the meander. For  $X < 1.5$ , we attribute the  $\sigma_{zm}$  reduction to the time averaging and estimate the time scale  $\tau_{im}$  of the meandering process from Eq. (1). Figure 12b shows that the  $\sigma_{zm}$  for the elevated source (red line) asymptotes to a linear dependence on  $X$  for  $X \ll 1$ , but with a reduced magnitude:  $\sigma_{zm} \simeq 0.65\sigma_{zmi}$ , where  $\sigma_{zmi}$  is the instantaneous meander. Using  $\sigma_{zm}/\sigma_{zmi} = 0.65$  in Eq. (1) and  $T_{av} = 1680$  s, we estimate a  $\tau_{im} = 0.21T_{av} = 355$  s or  $0.71z_i/w_*$ , which is a plausible value.

In air quality, a variable of much interest is  $\sigma_c/C$  and here we analyze a related variable—the CWIC fluctuation intensity  $\sigma_{C^y}/C^y$  at the surface. Figure 13a shows the LPDM-LES results for three source heights and the expected increase in  $\sigma_{C^y}/C^y$  with  $z_s$  at short range,  $X \leq 0.5$ . The increase is due to the meandering process, which leads to a  $\sigma_c/C$  increase in the plume tails (e.g., Sykes, 1988; Sawford and Stapountzis, 1986) and thus is greater for a more elevated source because the surface is farther removed from the plume centerline. For  $X > 1.5$ , the  $\sigma_{C^y}/C^y$  is essentially independent of source height because the elevated plume behaves like one from a surface release after plume “touchdown.” Figure 10 gives indirect support for the  $\sigma_{C^y}/C^y$  behavior for  $X > 0.3$  by the overlap of the LPDM-LES realizations with field data. For  $X < 0.3$ , the fluctuation intensity may be underestimated due to the neglect of relative dispersion ( $\sigma_r$ ) at short range, but the same qualitative dependence of  $\sigma_{C^y}/C^y$  on source height is expected with the use of  $\sigma_r$  from a 2-particle LPDM.



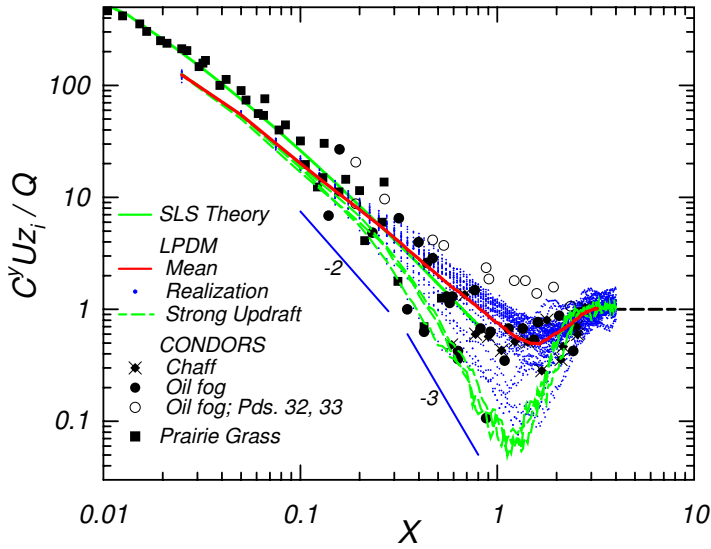
**Fig. 14** LPDM dimensionless plume height as a function of  $X$  for a surface source showing three strong updraft realizations, all other realizations (blue lines), and ensemble-mean height. Lines with slope  $\alpha = 1$  and  $3/2$  in  $\bar{z}_p/z_i \propto X^\alpha$  shown for reference.

Figure 13b provides some direct support for the LPDM in a comparison with the tank data of Hibberd (2000) for an elevated source ( $z_s/z_i = 0.25$ ). With the exception of the very near field ( $X < 0.25$ ), the two are in qualitative agreement with the LPDM (time-averaged) results falling below the laboratory data (short time-averages) as would be expected. In the near field, Hibberd reported some bias and uncertainty in the magnitude and location of the peak mean  $C^y$  relative to the WD78 data, and thus there is some uncertainty in his results close to the source.

#### 4.2.2 Yaglom's (1972) Theory for Mean Plume Height

In strong convection (e.g.,  $z_i/|L| > 50$ ), Yaglom (1972) argued that the buoyant production rate of turbulence,  $g\bar{w}\bar{\theta}_0/T_a$ , was the most important variable determining the mean rise rate of a plume from a surface source. Using dimensional reasoning, he predicted that the mean plume height varied as  $\langle \bar{z}_p \rangle \propto (g\bar{w}\bar{\theta}_0/T_a)^{1/2} t^{3/2}$  or  $\langle \bar{z}_p \rangle / z_i \propto X^{3/2}$ , but we are unaware of any plume height observations or numerical simulations demonstrating this scaling. Based on Yaglom's theory, Nieuwstadt (1980) reasoned that the vertical spread of a surface source should follow  $\sigma_z/z_i \propto X^{3/2}$  and that for a uniform wind, the surface CWIC would vary as  $C^y U z_i / Q \propto X^{-3/2}$ . His analysis of the Prairie Grass data verified this scaling for the mean CWIC although some of the data suggested an even steeper falloff of the CWIC with  $X$ .

Figure 14 shows a re-plot of the LPDM realizations and mean of  $\bar{z}_p/z_i$  versus  $X$  in logarithmic coordinates in order to determine the trajectory slope  $\alpha$  in  $\bar{z}_p/z_i \propto X^\alpha$ . The individual trajectories or realizations exhibit a range of slopes from  $\alpha \simeq 1$  to 1.5 and perhaps slightly greater, whereas the mean trajectory (red line) shows at most an  $\alpha \simeq 1.2$  over a short range of  $X$ . However, a few—up to 3 or 4—of the trajectories for strong updraft plumes exhibit a short range ( $0.1 < X < 0.4$ ) where  $\alpha \simeq 1.5$  and three are highlighted in Fig. 14 (green dashed lines). These are the strongest updraft cases in that the maximum  $\bar{z}_p$  is  $\geq 0.7z_i$  and larger than the maxima for the other realizations; one is the updraft plume in Fig. 2a.



**Fig. 15** Same as Fig. 10 but highlighting CWIC versus  $X$  profiles for three strong updraft plumes (green dashed lines), which are same cases denoted in Fig. 14. Lines with slope  $\beta = -2$  and  $-3$  in  $C^y U_{z_i} / Q \propto X^\beta$  shown for reference.

From these results, we conclude that a slope of 1.5 as predicted by Yaglom may exist for a few of the strongest updrafts, but the mean trajectory,  $\langle \bar{z}_p \rangle / z_i$  versus  $X$ , clearly does not have a slope that large. This probably occurs because more than 50% of the realizations are initially driven by downdrafts for which  $\alpha$  is closer to 1 (see Fig. 14; trajectories below the mean).

We note that these results may be dependent on the LES vertical grid resolution, which was  $\approx 21$  m. For this resolution, the surface layer ( $z \leq 0.1 z_i$ ) wherein the Yaglom (1972) theory is most applicable only contains five vertical grids. Thus, in future work it would be useful to repeat this analysis and others (e.g., the CWIC for a surface source) using a finer LES resolution.

#### 4.2.3 Variation of Surface CWIC with Distance for Surface Source in Very Unstable Conditions

Several authors analyzed the Prairie Grass surface CWIC data to infer the vertical dispersion rate for a surface source in very unstable conditions; e.g., Briggs (1982, 1978); Nieuwstadt (1980); Venkatram (1992). They characterized the stability and dispersion by different methods including MO similarity and SLS theory, eddy-diffusion, and convective scaling. They also proposed a variation of the mean surface CWIC as  $C^y \propto X^{-2}$ , which implies a faster dispersion or mean plume rise rate than given by the theory of Yaglom (1972) assuming  $U_p$  is constant. However, as noted earlier (Section 4.2.2), Nieuwstadt (1980) found that the PGr data plotted in convective scaling coordinates exhibited a mean CWIC variation as  $C^y \propto X^{-3/2}$ , and that the greater decrease in  $C^y$  with  $X$  found by the other authors was obscured by the data scatter.

In Fig. 15, we re-plot the dimensionless surface CWIC versus  $X$  for the surface source and highlight three strong updraft plumes (green dashed lines), the same three highlighted in Fig. 14. Over the range  $(0.1 < X < 0.3)$ , these cases exhibit an approximate  $X^{-2}$  behavior, but for larger  $X$  the variation is closer to  $C^y \propto X^{-3}$  before the CWIC “rebounds” towards the well-mixed result. Also note that the very low PGr and CONDORS measurements are consistent with these cases in lying along or close to the dashed lines. Further insight can be gained by examining the CWIC contours for the entire plume in Fig. 2a, which shows most of the plume being lofted temporarily into the upper reaches of the CBL (for  $X \leq 2$ ), leaving the surface “scalar deficient” with  $C^y U z_i / Q < 0.1$  in some places. However, for our ensemble of 30 realizations, the 3 or 4 strong updraft plumes exhibiting this behavior represent at most about 13% of all the realizations. Thus, they clearly do not represent the mean CWIC which follows an approximate  $C^y \propto X^{-3/2}$  behavior over the range  $0.2 < X < 1.4$ . These results are consistent with those of Nieuwstadt (1980).

## 5 Summary and Conclusions

We used a Lagrangian particle dispersion model (LPDM) driven by LES velocity fields to determine the mean and variability of plume dispersion in a highly convective PBL. In the LPDM (Weil et al, 2004), the total velocity of a wandering “particle” was divided into resolved and unresolved or random (subfilter scale, SFS) velocities with the resolved component obtained directly from the LES and the SFS velocity found from a Lagrangian stochastic model. The key new feature of this study was the calculation of the rms deviation and mean of dispersion properties from an ensemble of dispersion realizations, with each LPDM-LES realization being an average over a 28-min period. An ensemble of 30 realizations was developed for each of three source heights:  $z_s/z_i = 0, 0.07, \text{ and } 0.32$ . We compared the LPDM results with convection tank experiments, primarily those of Willis and Deardorff (1976) for  $z_s/z_i = 0.07$ , and field observations from the CONDORS and Prairie Grass experiments for  $z_s/z_i = 0$  and  $0.32$ .

The overarching conclusion is that the LPDM-LES model generates a realistic range of dispersion realizations and rms deviations that match observations in a highly convective PBL, while also matching the ensemble-mean properties. This conclusion holds for the plume height or trajectory, vertical dispersion, and the surface CWIC and their dependence on downstream distance. The results support John Wyngaard’s contention (Wyngaard, 1984) that LES is a powerful and useful approach for studying the statistical variability in dispersion and concentration variance. One exception is the crosswind dispersion for an elevated source, which is underestimated by the model and believed due to an underpredicted lateral variance and to wind direction shear. Some of the specific results and conclusions are summarized in the following.

For the near-surface source ( $z_s/z_i = 0.07$ ), the ensemble-mean CWIC contour field from the LPDM agreed well with that from the WD76 experiments in its overall shape and properties. It showed the rise or “lift-off” of the maximum CWIC from the surface, the temporary high CWICs in the upper part of the CBL, and the well-mixed scalar profile far downstream. Similar fields were shown for strong updraft- and downdraft-dominated plumes and demonstrated some key differences between them—the greater plume centerline tilt and higher CWICs aloft for the updraft plumes and the larger surface CWICs for the downdraft plumes. The variability in the CWIC profiles was initially greatest at the surface and close to the source, but by a dimensionless distance  $X \simeq 1.5$ , it was as large near the CBL top due to the superposition of CWICs from updraft- and downdraft-dominated plumes. Far down-

stream ( $X \simeq 3$ ), the variability decreased as the plume approached a vertically well-mixed state.

In the case of surface and elevated sources, the modeled mean, rms spread, and realization range of the average plume height ( $\bar{z}_p$ ), vertical dispersion ( $\sigma_z$ ), and surface CWICs agreed well with the CONDORS and Prairie Grass data. For  $\bar{z}_p$  and  $\sigma_z$ , the range of the realizations and their rms deviation included most of the CONDORS measurements and generally reproduced the shape of the data scatterband with  $X$ . For the surface source, there were exceptions for two observation periods of “squashed plumes” with unusually low  $\bar{z}_p$ 's. In addition, the LPDM mean dispersion for the elevated source matched the short-time statistical theory prediction,  $\sigma_z/z_i \simeq 0.6X$ , and it asymptoted to the expected value (0.29) for a well-mixed plume far downstream.

For the surface CWICs, the LPDM mean from the surface release agreed approximately with SLS theory for  $X < 0.5$  and followed  $C^y \propto X^{-3/2}$  over the range  $0.2 < X < 1.4$ , consistent with the results of Nieuwstadt (1980). Comparisons with the CONDORS and Prairie Grass data showed that for  $X > 0.3$ , most of the data were within the predicted rms deviation of the 30 realizations and almost all data fell within the range of the realizations. This was an important result and suggested that the turbulence variability from realization-to-realization was the primary cause of the observed CWIC variability. For the elevated source, the mean CWIC exhibited the familiar increase to a maximum value similar to results obtained by WD78 and Lamb (1978). An important new result was the computed variability in the CWIC which ranged over two orders of magnitude near the source ( $X < 0.4$ ) and was attributed to the meandering of the elevated plume by the large CBL eddies.

With the lateral dispersion ( $\sigma_y$ ), the modeled mean  $\sigma_y$  for a surface source asymptoted to  $\sigma_y/z_i = X$  at short range ( $X \ll 1$ ) in agreement with the CONDORS and Prairie Grass data and tended towards an  $X^{1/2}$  behavior for large  $X$  ( $> 1$ ). The small  $X$  result, with a coefficient of 1 rather than 0.6 on the right-hand-side, was due to the increased  $\sigma_y$  and reduced wind near the surface. Both the small- and large- $X$  behaviors were consistent with predictions from the statistical theory of dispersion. Nearly all of the observations fell within the range of the LPDM realizations for the surface source but for the elevated source, the LPDM underestimated the lateral dispersion and variability for the reasons discussed above.

Other analyses highlighted important LPDM results on: 1) the plume meander and CWIC fluctuation intensity at the surface, 2) the applicability of similarity theory (Yaglom, 1972) for plume height from a surface source to only the very strong updraft plumes (i.e., not the mean height), and 3) the appropriate variation with distance of  $C^y$  and the lower bound of the surface CWIC realizations for a surface source.

**Acknowledgements** We thank John Wyngaard for his inspirations, many collaborations over the years, and for being a colleague, mentor, and friend. This work was supported by the U.S. Army Research Office under Grant No. W911NF-09-1-0572 with Dr. Walter D. Bach as the program manager during the course of the research. J.C. Weil also is grateful to the U.S. Defense Threat Reduction Agency for partial support during the data analysis and preparation of this paper. We thank two anonymous reviewers for helpful comments.

## References

Barad ML (1958) Project Prairie Grass. A field program in diffusion. Geophysical Research Paper No. 59, Vols. I and II AF-CRF-TR-235, Air Force Cambridge Research Center, Bedford, MA

- Briggs GA (1978) Prairie grass revisited. optimum indicators of vertical spread. In: Proceedings 9th Int. Technical Meeting on Air Pollution and its Application, NATO/CCMS, pp 209–220
- Briggs GA (1982) Similarity forms for ground-source surface-layer diffusion. *Boundary-Layer Meteorol* 23:489–502
- Briggs GA (1993) Plume dispersion in the convective boundary layer. Part II: Analyses of CONDORS field experiment data. *J Appl Meteorol* 32:1388–1425
- Caughy SJ (1982) Observed characteristics of the atmospheric boundary layer. In: Nieuwstadt F, van Dop H (eds) *Atmospheric Turbulence and Air Pollution Modelling*, Reidel, Dordrecht, Holland, pp 107–159
- Csanady GT (1973) *Turbulent Diffusion in the Environment*. Reidel
- Deardorff JW (1972) Numerical investigation of neutral and unstable planetary boundary layers. *J Atmos Sci* 29:91–115
- Deardorff JW, Willis GE (1984) Groundlevel concentration fluctuations from a buoyant and a non-buoyant source within a convectively mixed layer. *Atmos Environ* 18:1297–1309
- Deardorff JW, Willis GE (1988) Concentration fluctuations within a laboratory convective planetary boundary layer. In: Venkatram A, Wyngaard JC (eds) *Lectures on Air Pollution Modeling*, American Meteorological Society, Boston, MA, pp 357–384
- Dosio A, de Arellano JVG (2006) Statistics of absolute and relative dispersion in the atmospheric convective boundary layer: a large-eddy simulation study. *J Atmos Sci* 63:1253–1272
- Dosio A, de Arellano JVG, Holtslag AAM, Builtjes PJH (2003) Dispersion of a passive tracer in buoyancy- and shear-driven boundary layers. *J Appl Meteorol* 42:1116–1130
- Eberhard WL, Moninger WR, Briggs GA (1988) Plume dispersion in the convective boundary layer. Part I: CONDORS field experiment and example measurements. *J Appl Meteorol* 27:599–616
- Fox DG (1984) Uncertainty in air quality modeling. *Bull Amer Meteorol Soc* 65:27–36
- Gifford FA (1959) Statistical properties of a fluctuating plume dispersion model. In: *Advances in Geophysics*, vol 6, Academic Press, pp 117–138
- Hanna SR, Paine RJ (1989) Hybrid plume dispersion model (HPDM) development and evaluation. *J Appl Meteorol* 28:206–224
- Henn DS, Sykes RI (1992) Large-eddy simulation of dispersion in the convective boundary layer. *Atmos Environ* 26a:3145–3159
- Hibberd M (2000) Vertical dispersion of a passive scalar in the convective boundary layer: new laboratory results. In: *Preprints, 11th Joint Conference on the Applications of Air Pollution Meteorology with the A & WMA*, American Meteorological Society, Long Beach, CA, pp 18–23
- Hicks BB (1985) Behavior of turbulent statistics in the convective boundary layer. *J Clim Appl Meteorol* 24:607–614
- Horst TW (1979) Lagrangian similarity modeling of vertical diffusion from a ground-level source. *J Appl Meteorol* 18:733–740
- Lamb RG (1978) A numerical simulation of dispersion from an elevated point source in the convective planetary boundary layer. *Atmos Environ* 12:1297–1304
- Lamb RG (1982) Diffusion in the convective boundary layer. In: Nieuwstadt F, van Dop H (eds) *Atmospheric Turbulence and Air Pollution Modelling*, Reidel, Dordrecht, Holland, pp 159–229
- Lewellen WS, Sykes RI (1986) Analysis of concentration fluctuations from lidar observations of atmospheric plumes. *J Clim Appl Meteorol* 25:1145–1154

- Luhar AK, Hibberd MF, Borgas MS (2000) A skewed meandering plume model for concentration statistics in the convective boundary layer. *Atmos Environ* 34:3599–3616
- Lumley JL, Panofsky HA (1964) *The Structure of Atmospheric Turbulence*. Wiley Interscience
- Moeng CH (1984) A large-eddy simulation model for the study of planetary boundary-layer turbulence. *J Atmos Sci* 41:2052–2062
- Moeng CH, Sullivan PP (1994) A comparison of shear- and buoyancy-driven planetary boundary layer flows. *J Atmos Sci* 51:999–1022
- Moeng CH, Wyngaard JC (1988) Spectral analysis of large-eddy simulations of the convective boundary layer. *J Atmos Sci* 45:3573–3587
- Mylne KR, Mason PJ (1991) Concentration fluctuation measurements in a dispersing plume at a range of up to 1000m. *Quart J Roy Meteorol Soc* 117:177–206
- Nieuwstadt FTM (1980) Application of mixed-layer similarity to the observed dispersion from a ground-level source. *J Appl Meteorol* 19:157–162
- Nieuwstadt FTM (1992) A large-eddy simulation of a line source in a convective atmospheric boundary layer—I. Dispersion characteristics. *Atmos Environ* 26A:485–495
- Nieuwstadt FTM, Mason PJ, Moeng CH, Schumann U (1993) Large-eddy simulation of the convective boundary layer: A comparison of four computer codes. In: Durst F, Friedrich R, Launder BE, Schmidt FW, Schumann U, Whitelaw JH (eds) *Turbulent Shear Flows 8*, Springer-Verlag, Berlin
- Sawford BL, Guest FM (1987) Lagrangian stochastic analysis of flux-gradient relationships in the convective boundary layer. *J Atmos Sci* 44:1152–1165
- Sawford BL, Stapountzis H (1986) Concentration fluctuations according to fluctuating plume models in one and two dimensions. *Boundary-Layer Meteorol* 37:89–105
- Smith FB (1965) The role of wind shear in horizontal diffusion of ambient particles. *Quart J Roy Meteorol Soc* 91:318–329
- Snyder WH, Lawson REJ, Shipman RE, Lu J (2002) Fluid modelling of atmospheric dispersion in the convective boundary layer. *Boundary-Layer Meteorol* 102:335–366
- Sykes RI (1988) Concentration fluctuations in dispersing plumes. In: Venkatram A, Wyngaard JC (eds) *Lectures on Air Pollution Modeling*, American Meteorological Society, Boston, MA, pp 325–356
- Taylor GI (1921) Diffusion by continuous movements. *Proc London Math Soc* 20:196–211
- Thomson DJ (1987) Criteria for the selection of stochastic models of particle trajectories in turbulent flows. *J Fluid Mech* 180:529–556
- Thomson DJ (1990) A stochastic model for the motion of particle pairs in isotropic high Reynolds number turbulence, and its application to the problem of concentration variance. *J Fluid Mech* 210:113–153
- van Ulden AAP (1978) Simple estimates for vertical diffusion from sources near the ground. *Atmos Environ* 12:2125–2129
- Venkatram A (1988a) Dispersion in the stable boundary layer. In: Venkatram A, Wyngaard JC (eds) *Lectures on Air Pollution Modeling*, American Meteorological Society, Boston, MA, pp 229–265
- Venkatram A (1988b) Topics in applied dispersion modeling. In: Venkatram A, Wyngaard JC (eds) *Lectures on Air Pollution Modeling*, American Meteorological Society, Boston, MA, pp 267–324
- Venkatram A (1992) Vertical dispersion of ground-level releases in the surface boundary layer. *Atmos Environ* 26A:947–949
- Weil JC (1985) Updating applied diffusion models. *J Clim Appl Meteorol* 24:1111–1130

- 
- Weil JC (1988) Dispersion in the convective boundary layer. In: Venkatram A, Wyngaard JC (eds) *Lectures on Air Pollution Modeling*, American Meteorological Society, Boston, MA, pp 167–227
- Weil JC (1990) A diagnosis of the asymmetry in top-down and bottom-up diffusion using a Lagrangian stochastic model. *J Atmos Sci* 47:501–515
- Weil JC, Sykes RI, Venkatram A (1992) Evaluating air-quality models: Review and outlook. *J Appl Meteorol* 31:1121–1145
- Weil JC, Snyder WH, Lawson RE, Shipman MS (2002) Experiments on buoyant plume dispersion in a laboratory convection tank. *Boundary-Layer Meteorol* 102:367–414
- Weil JC, Sullivan PP, Moeng CH (2004) The use of large-eddy simulations in Lagrangian particle dispersion models. *J Atmos Sci* 61:2877–2887
- Willis GE, Deardorff JW (1976) A laboratory model of diffusion into the convective planetary boundary layer. *Quart J Roy Meteorol Soc* 102:427–445
- Willis GE, Deardorff JW (1978) A laboratory study of dispersion from an elevated source within a modeled convective planetary boundary layer. *Atmos Environ* 12:1305–1312
- Willis GE, Deardorff JW (1981) A laboratory study of dispersion from an elevated source within a modeled convective planetary boundary layer. *Atmos Environ* 15:109–117
- Wilson JD, Sawford BL (1996) Review of Lagrangian stochastic models for trajectories in the turbulent atmosphere. *Boundary-Layer Meteorol* 78:191–220
- Wyngaard JC (1973) On surface layer turbulence. In: Haugen DA (ed) *Workshop on Micrometeorology*, American Meteorological Society, Boston, MA, pp 101–149
- Wyngaard JC (1984) Large-eddy simulation: Guidelines for its application to planetary-boundary layer research. Tech. Rep. 0804, US Army Research Office
- Wyngaard JC (1985) Structure of the planetary boundary layer and implications for its modeling. *J Clim Appl Meteorol* 24:1131–1142
- Wyngaard JC (1988) Structure of the PBL. In: Venkatram A, Wyngaard JC (eds) *Lectures on Air Pollution Modeling*, American Meteorological Society, Boston, MA, pp 9–61
- Yaglom AM (1972) Turbulent diffusion in the surface layer of the atmosphere. *Izv Akad Nauk USSR, Atmos Ocean Phys* 8:333–340